

---

# Quantification of [<sup>18</sup>F]FDG Uptake in the Normal Liver Using Dynamic PET: Impact and Modeling of the Dual Hepatic Blood Supply

Gunnar Brix, Sibylle I. Ziegler, Matthias E. Bellemann, Josef Doll, Rudolph Schosser, Robert Lucht, Heiner Krieter, Dietmar Nosske, and Uwe Haberkorn

*Research Program Radiological Diagnostics and Therapy, German Cancer Research Center, Heidelberg; Department of Experimental Surgery, University of Heidelberg, Heidelberg; Department of Medical Radiation Hygiene, Institute of Radiation Hygiene, Federal Office for Radiation Protection, Neuherberg; Department of Nuclear Medicine, Technische Universität München, Munich; and Department of Biomedical Engineering, University of Applied Sciences, Jena, Germany*

For quantification of hepatic [<sup>18</sup>F]FDG uptake, the dual blood supply to the liver must be considered. In contrast to the arterial input, however, the portal venous blood supply to the liver cannot be monitored directly by PET because of the inaccessibility of the portal vein on PET scans. In this study, we investigated whether the dual hepatic input can be predicted from the measurable arterial input. Moreover, we assessed the effect of different input models on the rate constants of the standard 3-compartment model describing regional uptake of FDG. **Methods:** Dynamic FDG PET scanning was performed on 5 foxhounds. Activity concentrations in blood from the aorta and the portal vein were measured simultaneously using external circuits. After image reconstruction, time-activity courses were determined from the aorta and the liver. The venous input was approximated by convolving the arterial input with a notional system function describing the dispersion of the arterial input on its way through the gastrointestinal tract. On the basis of these data, 5 different hepatic input models, which pertain to a single-input as well as a dual-input scenario, were statistically compared with regard to the adequacy of the model fits to liver data and to differences in the estimated rate constants. **Results:** Portal venous input to the liver could be approximated by convolving the arterial input function with a system function. From this function, a mean transit time of 25 s was computed for FDG to pass through the gastrointestinal tract. According to the statistical analysis, dual-input models were superior to their single-input counterparts. However, differences in the rate constants estimated for the 5 input models were in the same order as interindividual variations within the different model groups. For the dephosphorylation rate constant, a consistent value of  $0.05 \pm 0.01 \text{ min}^{-1}$  was found. **Conclusion:** Dual-input models proved to be superior to single-input models with respect to the adequacy of FDG model fits to normal liver data. However, the hepatic blood supply may be approximated by the arterial input function as

well, especially for the evaluation of liver lesions mainly fed by the hepatic artery.

**Key Words:** PET; liver tissue; dual hepatic blood supply; FDG modeling

**J Nucl Med** 2001; 42:1265–1273

---

## T

The role of PET with the radiolabeled glucose analog [<sup>18</sup>F]FDG in the detection and characterization of malignant tumors and other diseases of the liver has been investigated recently in several clinical studies (1–8). These studies have shown that the detection of liver tumors and especially of benign lesions with FDG PET is hampered by the fact that FDG uptake in many lesions is at the same level as in healthy liver tissue. This finding is explained by the relatively high FDG uptake in normal liver tissue and the variable accumulation of FDG in liver tumors because of their varying degree of activity of the enzyme glucose-6-phosphatase (9,10). However, evaluation of liver tumors—especially of hepatocellular carcinoma—may be improved by dynamic FDG PET measurements and the computation of parametric images characterizing FDG transport and metabolism.

This approach, however, requires that the time-activity course of unmetabolized tracer delivered to the liver (i.e., the input function) must be determined in each subject. In contrast to other organs or tissues, which are supplied only by arterial blood, the liver has a dual blood supply comprising the hepatic artery delivering blood from the heart and the portal vein delivering venous blood that drains the gastrointestinal tract. In human subjects, the portal vein supplies about 75% of the hepatic vascular input and the hepatic artery supplies about 25% (11). This fact has to be considered when FDG kinetics in the liver are to be determined with compartment models. There are 2 solutions to this problem: The first is the direct measurement of the dual hepatic blood supply by cannulation of the hepatic artery

---

Received Oct. 30, 2000; revision accepted Apr. 12, 2001.

For correspondence or reprints contact: Gunnar Brix, PhD, Institut für Strahlenhygiene, Bundesamt für Strahlenschutz, Ingolstädter Landstrasse 1, 85764 Neuherberg, Germany.

and portal vein to obtain the arterial input and the portal venous input, respectively. However, this procedure is only applicable for laboratory animals or after surgical intervention in humans. Second is the approximation of the portal venous input from the arterial input, which can be determined, for example, by arterial or arterialized venous blood sampling as well as directly from a large artery or the left ventricle as visualized on the PET scans. The second approach was used, for example, by Choi et al. (12), who assumed that the dual blood supply to the liver could be approximated by the arterial input with a finite time delay because FDG extraction in portal circulation should be small and a major portion of FDG is delivered through the portal vein. In combination with a 3-compartment model, these authors obtained an adequate parameterization of measured liver data. This approach, however, does not show that the estimated model parameters are correct.

This study had 3 aims: to directly measure the arterial and portal venous blood activity in foxhounds as a function of time, to investigate whether the portal venous input can be estimated from the measured arterial input, and to examine in normal liver tissue the effect of different input models on pharmacokinetic parameter estimates for the standard 3-compartment FDG model.

## MATERIALS AND METHODS

### Animal Preparation

Experimental handling of the animals was performed in accordance with the guidelines described in the German Protection of Animals Act. Five FDG studies were performed on foxhounds (23–30 kg) lying in the supine position. Each experiment comprised a PET study together with the extracorporeal measurement of the activities in arterial and venous blood feeding the liver. Before the examination, the dogs were subjected to fasting for 24 h, premedicated with intramuscular propiomypromazine (Combelen [1.5–3.0 mL/kg]; Bayer, Leverkusen, Germany), and anesthetized with intravenous pentobarbital (Nembutal [15 mg/kg]; Ceva, Bad Segeberg, Germany) and alcuronium (Alloferin [0.25 mg/kg]; Roche, Grenzach-Wyhlen, Germany) for neuromuscular blocking. The animals were intubated and mechanically ventilated using a volume-controlled respirator (SERVO 900 C; Siemens-Elma, Solna, Sweden) operating with a mixture of 35% O<sub>2</sub> and 65% N<sub>2</sub>O at a rate of 12 breaths per minute and an initial tidal volume of 150 mL/kg. Body temperature was maintained at 37°C ± 1°C by placing the dogs on a heated pad. Infusion of 8.4% NaHCO<sub>3</sub> was used to compensate for metabolic acidosis.

For the injection of radiolabeled FDG, a peripheral vein was cannulated. In addition, a catheter was inserted through the right carotid artery into the aorta to measure arterial blood activities during PET scanning. A 5- to 10-cm median laparotomy incision was made, and a thin catheter was introduced into a venous side branch and advanced to the distal part of the portal vein to provide a measure of the venous input to the liver.

The dogs were hemodiluted with 6% dextran 60 (Macrodex; Schodia, Glandorf, Germany) to a hematocrit of 0.30 and allowed to stabilize for 30 min. For the radiotracer measurements, anesthesia was maintained by continuous infusion of piritramide (Dipidolor; Janssen, Neuss, Germany) at a rate of 0.45 mg/kg/h. To

maintain a constant end-expiratory concentration of 1.2% volume, isoflurane (Florene; Abbott, Wiesbaden, Germany) was added to the inspiratory gas flow.

### Radiotracer Measurements

Immediately after the administration of 102–140 MBq FDG (13) into the peripheral vein of the dogs, the regional FDG uptake was observed with a whole-body scanner (PC 2048-7WB; Scanditronix, Uppsala, Sweden (14)) over a period of 60 min by measuring eight 30-s frames followed by six 60-s frames and ten 300-s frames. Blood activities in the aorta and the portal vein were monitored simultaneously by continuously withdrawing blood at a constant rate of 3 mL/min through tubing of 1-mm diameter and measuring the counting rate in 2 independent coincidence-based detector systems (fluid monitors; 1 Scanditronix Bi<sub>4</sub>Ge<sub>3</sub>O<sub>12</sub> system (15) and 1 NaI laboratory design system) with a temporal resolution of 1 s. The blood was recirculated through the left femoral vein. Additional blood samples (0.5 mL) were taken 3.5 min after beginning the scanning procedure at each of the detector sites, measured in a well counter, and used to calibrate the detector systems. The calibrated blood activity curves were decay corrected to the time of injection.

Before emission scanning, a 10-min transmission scan was acquired using a <sup>68</sup>Ge rod source. The emission sinograms with 256 projections of 256 members each were corrected subsequently for scattered radiation (16) and attenuation. PET images (matrix size, 256 × 256; pixel size, 2 × 2 mm<sup>2</sup>) were generated by use of an iterative maximum-likelihood algorithm with successive over-relaxation for accelerated convergence (17) on a DEC 3000/400 AXP workstation (Digital Equipment Corp., Maynard, MA).

For quantitative analysis, regions of interest (ROIs) were defined over the right and left side of the liver as well as over the central part of the aorta. Time–activity curves were created by averaging the activity in each region on a frame-by-frame basis, decay corrected to the time of injection, and calibrated. To correct for underestimation of activity concentrations in the aorta associated with the limited spatial resolution of the PET scanner, a recovery coefficient of 0.78 was estimated from values reported for the PC 2048-7WB scanner (17) assuming a mean diameter of 11 mm for the aorta as determined from MR angiograms of 3 foxhounds (18). Following the approach usually used in clinical PET, all activity concentrations were normalized to the injected FDG dose and the body weight of the animals, yielding standardized uptake values (SUVs): SUV<sub>arterial</sub><sup>detector</sup>, SUV<sub>venous</sub><sup>detector</sup>, SUV<sub>aorta</sub><sup>PET</sup>, and SUV<sub>liver</sub><sup>PET</sup>. By this approach, it is possible to compare the input functions and the FDG uptake curves in the liver among the foxhounds.

### Input Functions

To examine whether the dual blood supply to the liver could be predicted if only the arterial input is known, the portal venous input was described by convolution of the arterial input with a notional system function:

$$S(t) = t^{P_0} [P_1 \cdot \exp(-P_2 \cdot t) + P_3 \cdot \exp(-P_4 \cdot t)], \quad \text{Eq. 1}$$

which is a combination of 2 gamma variate functions commonly used in tracer kinetic modeling to describe the dispersion of an arterial input on its way through an organ or a tissue (11). The 5 model parameters P<sub>0</sub>, P<sub>1</sub>, P<sub>2</sub>, P<sub>3</sub>, and P<sub>4</sub> were computed for each dog from the individual SUV<sub>arterial</sub><sup>detector</sup> and SUV<sub>venous</sub><sup>detector</sup> curves by nonlinear least-squares fits performed on a personal computer (Pen-

tium Pro [200 MHz]; Intel, Feldkirchen, Germany) using the program IDL (Interactive Data Language, Version 5.2; Research Systems, Boulder, CO). Moreover, an average system function,  $\bar{S}$ , was estimated from the mean arterial and the mean portal venous function, which were derived by averaging over the individual input functions.

Because the hepatic arterioles and the portal venules anastomose and completely mix proximal to the sinusoid, the nutrient vessel within the liver, the 2 inputs can be combined to form a unique input function for pharmacokinetic modeling (11). The relative weights of the arterial and portal venous blood supply are given by the relative inflow values. For the same foxhounds, Ziegler et al. (19) reported mean hepatic artery and portal venous blood flow values of 0.33 and 0.60 mL/min/g, respectively, which correspond to relative weighting factors of  $w_{arterial} = 0.35$  and  $w_{venous} = 0.65$ .

On the basis of these considerations, 5 different hepatic input functions were created for each dog:

$$SUV_{in}^{#1} = w_{arterial} \cdot SUV_{arterial}^{detector} + w_{venous} \cdot SUV_{venous}^{detector}, \quad \text{Eq. 2}$$

$$SUV_{in}^{#2} = SUV_{arterial}^{detector}, \quad \text{Eq. 3}$$

$$SUV_{in}^{#3} = w_{arterial} \cdot SUV_{arterial}^{detector} + w_{venous} \cdot \bar{S} \otimes SUV_{arterial}^{detector}, \quad \text{Eq. 4}$$

$$SUV_{in}^{#4} = SUV_{arterial}^{PET}, \quad \text{Eq. 5}$$

$$SUV_{in}^{#5} = w_{arterial} \cdot SUV_{arterial}^{PET} + w_{venous} \cdot \bar{S} \otimes SUV_{arterial}^{PET}. \quad \text{Eq. 6}$$

Input function #1 is the weighted sum of the measured arterial and portal venous blood activities and served as a reference function. Functions #2 and #4 approximate the hepatic blood supply by means of the arterial activity values obtained from the external detector system and from dynamically acquired PET scans, respectively. This approach corresponds to the single-input model used by Choi et al. (12). In contrast, input functions #3 and #5 pertain to a dual-input scenario where the portal venous input is estimated by convolution (which is denoted by the symbol  $\otimes$  in Equations 4 and 6) of the measured arterial input with the average system function  $\bar{S}$ .

The FDG time–activity courses in blood plasma were determined from the corresponding whole blood curves by applying a 2-compartment model describing the exchange of FDG between plasma and erythrocytes. The rate constants describing the exchange processes were obtained in a previous experimental study with rats (20,21), in which we found an influx rate of FDG into erythrocytes of  $0.06 \text{ min}^{-1}$  and an outflux rate of  $0.09 \text{ min}^{-1}$ . Because the glucose transporter isoform 1, which is responsible for glucose transport in erythrocytes, is highly conserved between the different mammalian species, similar influx and outflux rates can be assumed for rat and dog erythrocytes.

### Pharmacokinetic Analysis

A 3-compartment pharmacokinetic model (22,23) was used for assessment of FDG transport and metabolism in the liver. It consisted of 3 compartments describing FDG in arterial blood plasma, FDG in tissue, and FDG-6-phosphate in tissue. The model configuration was realized within the ADAPT II program environment (24) on a DEC PW 500au workstation (Digital Equipment Corp.) and included nonlinear least-squares fitting for parameter estimation. The rate constants that describe the compartmental fluxes include  $K_1$  (mL/min/g) and  $k_2$  ( $\text{min}^{-1}$ ) for forward and

backward transport of FDG, respectively. The rate constants  $k_3$  ( $\text{min}^{-1}$ ) and  $k_4$  ( $\text{min}^{-1}$ ) refer to the phosphorylation of FDG and the dephosphorylation of FDG-6-phosphate in the liver, respectively. The model configuration included 2 additional parameters: a blood volume fraction,  $f_B$ , to account for nonextracted FDG activity remaining within the vascular space of liver tissue and a lag time to correct for the time delay of FDG activity arrival in the extracorporeal detector loops. Because tubing and flow rate were identical for both extracorporeal loops, the same time delay was used for the arterial and the portal venous blood supply.

### Statistical Analysis

To statistically compare the adequacy of the model fits to the liver data by using the different input functions defined by Equations 2–6, the Schwarz criterion  $SC = N \ln(SS) + P \ln(N)$  (25) was computed for each case, where  $SS$  is the residual weighted sum of squares between measured and fitted liver data,  $N$  is the number of data points, and  $P$  is the number of model parameters. Model fits with a low  $SC$  are preferred.

For each fit parameter, the data analysis yielded for each of the 5 dogs an independent block of data with 5 parameter estimates relating to the different input models defined by Equations 2–6. The null hypothesis, that there is no effect of the input model on the rate constants, was tested separately for each fit parameter by means of Friedman's rank test for related samples (26) at a significance level of  $P = 0.05$ . When the null hypothesis was rejected, a rank test described by Wilcoxon and Wilcox (26,27) was used at the same significance level for comparisons between pairs of related parameter distributions.

## RESULTS

The extensive measurement protocol described could be conducted successfully on all 5 dogs. Two representative frames from a dynamic PET study are shown in Figure 1. On the PET scan acquired during the early perfusion phase, the aorta is well delineated. Therefore, time–activity courses could be derived from the aorta by placing an ROI over the central part of the vessel. The image acquired during the metabolic phase shows homogeneous FDG uptake across the liver. Because this observation applied also for the other PET frames, time–activity courses obtained from the right and left side of the liver were averaged before pharmacokinetic modeling.

Typical blood time–activity courses determined in the aorta and the portal vein of foxhound 4 are shown in Figure 2. The 3 time–activity courses, which were obtained by the 2 external detector systems ( $SUV_{arterial}^{detector}$ ,  $SUV_{venous}^{detector}$ ) and from the dynamically acquired PET scans ( $SUV_{aorta}^{PET}$ ) agreed very well with each other at the end of the measuring period. This result proves that the 3 measurement devices were calibrated correctly. Moreover, the courses reveal that 2 different dispersion effects must be considered: Because the arterial input function measured by the external detector system ( $SUV_{arterial}^{detector}$ ) was (for all dogs) broader than the arterial input function obtained from the PET images ( $SUV_{aorta}^{PET}$ ), the input is dispersed on its way through the external catheter system. In addition, the peak region for the portal venous function ( $SUV_{venous}^{detector}$ ) is spread out markedly

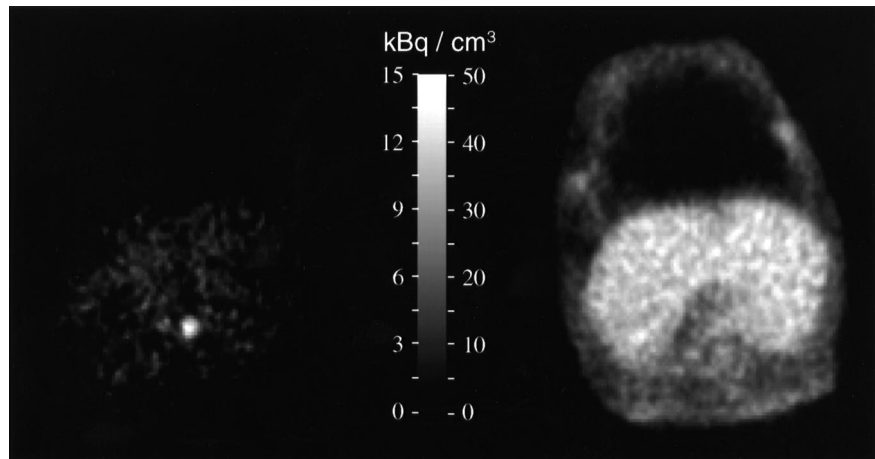


**FIGURE 1.** Representative PET scans show FDG distribution in a foxhound 0.25 min (frame 1, left) and 12.5 min (frame 15, right) after intravenous FDG administration. Time-activity courses were derived from ROIs defined over aorta and over right and left side of liver.

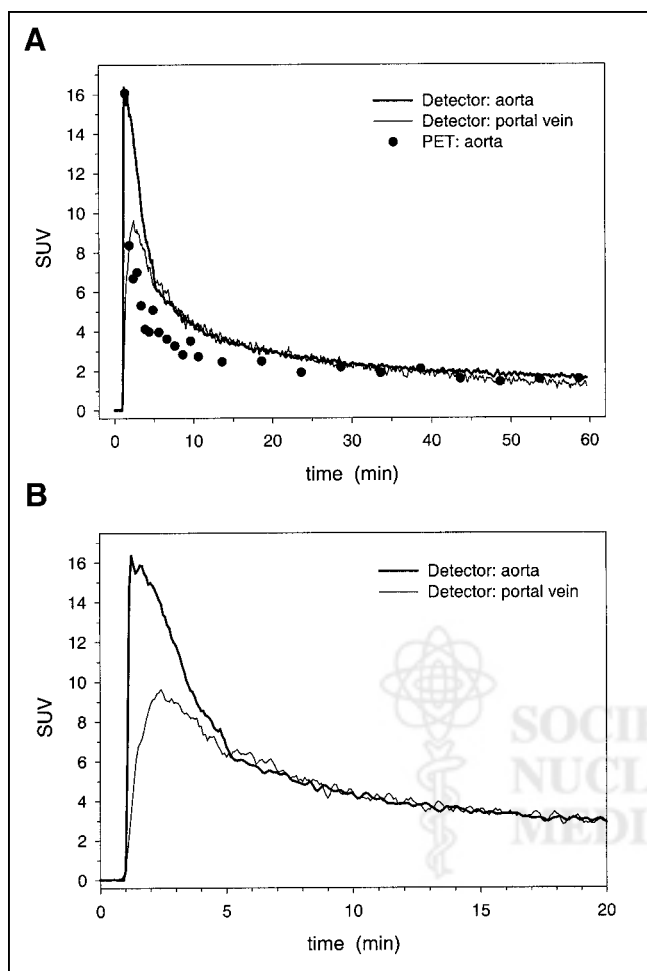


**FIGURE 2.** (A) Typical blood activity curves determined in aorta and portal vein of foxhound 4. Data were determined simultaneously by 2 independent detector systems (fluid monitors) with temporal resolution of 1 s and directly from aorta visualized on PET scans (Fig. 1, left). For better comparison, PET curve was shifted so that its maximum aligns with maximum of arterial blood curve measured by fluid monitor. (B) Detail of A, which shows that initial part of portal input is characterized by much lower maximum activity concentration and later moment of maximum concentration relative to arterial input.

compared with the 2 arterial functions because of a dispersion of the arterial input on its way through the gastrointestinal tract to the portal vein.

To analytically describe the “physiologic” dispersion effect, it was assumed that the dispersion of the arterial and portal venous input function in the extracorporeal detector loops is almost identical and that the portal venous function can thus be approximated by a convolution of the arterial input function with the notional system function  $S$  defined in Equation 1. The 5 model parameters fitted for each dog from the individual arterial and portal venous input functions are summarized in Table 1, which also gives the parameters derived from the mean time-activity courses averaged over the individual animal data. The average system function  $\bar{S}$  is plotted in Figure 3. It reveals that the system function is dominated by 1 of the 2 gamma variate functions defined in Equation 1—namely, by the fast component  $S_f(t) = t^{P_0} \cdot P_1 \cdot \exp(-P_2 \cdot t)$ . In spite of this fact, however, the second gamma variate function is necessary to achieve an adequate approximation of the measured data. In contrast to the parameters  $P_0$ ,  $P_3$ , and  $P_4$ , there is a large interindividual variation in the estimates for the parameters  $P_1$  and  $P_2$ , describing the shape of the fast component of the system function. However, both parameters are strongly correlated, and thus the variation in the shape of the individual system functions is much smaller than the variation in the individual fit parameters. This is verified by the fact that the mean transit time  $MTT_f$  of the fast component, which is defined as the first moment of the fast component of the system function, varies only between 13.1 and 34.6 s (Table 1).

As shown in Figure 4 on the basis of the example of dog 4, convolution of the externally measured arterial input function with the individual and the average system function resulted in a suitable approximation of the portal venous input function measured directly by the external detector system. The approximation of the portal venous input by convolution of the arterial input derived from the PET scans with the average system function resulted in a markedly sharper peak region.

**TABLE 1**  
Fit Parameters of System Function as Defined in Equation 1 Estimated for 5 Foxhounds

Dog no.	$P_0$	$P_1$	$P_2$ ( $\text{min}^{-1}$ )	$P_3$	$P_4$ ( $\text{min}^{-1}$ )	$\chi^2_{\text{ind}}^*$	$\chi^2_{\text{ave}}^*$	$MTT_f^{\dagger}$ (s)
1	1.92	9.19	6.79	$0.71 \cdot 10^{-3}$	0.37	52.3	88.4	18.7
2	1.40	15.6	10.0	$0.59 \cdot 10^{-3}$	0.35	12.3	235.9	13.1
3	1.45	1.80	4.20	$0.50 \cdot 10^{-3}$	0.35	27.7	46.3	31.2
4	1.74	3.18	5.11	$0.70 \cdot 10^{-3}$	0.35	62.5	75.9	24.0
5	1.78	0.76	3.28	$0.71 \cdot 10^{-3}$	0.35	22.2	434.6	34.6
Average curve	1.74	3.35	5.09	$0.60 \cdot 10^{-3}$	0.35	176	—	25.3

\* Residual sum of squares between measured and calculated portal venous activity values.  $\chi^2_{\text{ind}}$  and  $\chi^2_{\text{ave}}$  characterize approximation of portal venous function by convolution of arterial input function with corresponding individual system function and average system function, respectively.

† Mean transit time of dominant fast component  $S_f(t) = t^{P_0} \cdot P_1 \cdot \exp(-P_2 \cdot t)$  of estimated system function.

Parameters were estimated by means of nonlinear least-squares fit for each dog from individual arterial and portal venous input functions as well as from averaged time-activity courses. Errors in fit parameters were <1.5%.

For the same dog, the hepatic input functions computed for the 5 different input models defined by Equations 2–6 are plotted in Figure 5. The shape of the hepatic input functions #2 and #4, which correspond to the single-input model, in which the hepatic blood supply is described solely by the arterial input, deviates considerably from the shape of the input functions pertaining to the dual-input approach. The corresponding model fits to the time-activity course determined from the liver of dog 4 ( $SUV_{\text{liver}}^{\text{PET}}$ ) are shown in Figure 6.

For nonlinear least-squares fitting of the rate constants as defined by the standard 3-compartment FDG model, we used an initial value for the blood volume fraction of  $f_B = 0.28$  derived from the literature (28). For 22 of 25 curve fits (5 liver curves with 5 different input functions each),  $f_B$  was fitted to zero. In the other 3 cases, the analysis yielded a

nonzero but very low value of  $f_B < 5.7\%$ . This result is congruent with the observation that the liver curves did not show a prominent peak during the early perfusion phase (compare Fig. 6 with Fig. 5). Consequently, all fits were repeated with a blood volume fraction fixed to zero to improve the reliability of the estimates for the remaining parameters.

The rate constants obtained by this approach are plotted in Figure 7 for the 5 input models investigated. The relative mean fit errors in the final estimates were 5.9% for  $K_1$ , 8.5% for  $k_2$ , 35.1% for  $k_3$ , and 39.4% for  $k_4$ . By applying Friedman's rank test for related samples, the null hypothesis that there is no effect of the different input models on the estimated fit parameters could be rejected ( $P < 0.05$ ) for

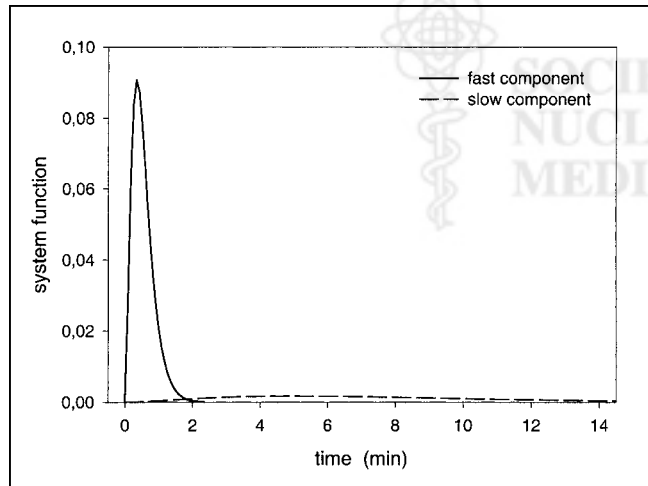


**FIGURE 3.** Fast and slow component of average system function  $\bar{S}$  approximating dispersion of arterial input on its way through gastrointestinal tract to portal vein in 5 foxhounds. Corresponding fit parameters estimated according to Equation 1 are summarized in Table 1.

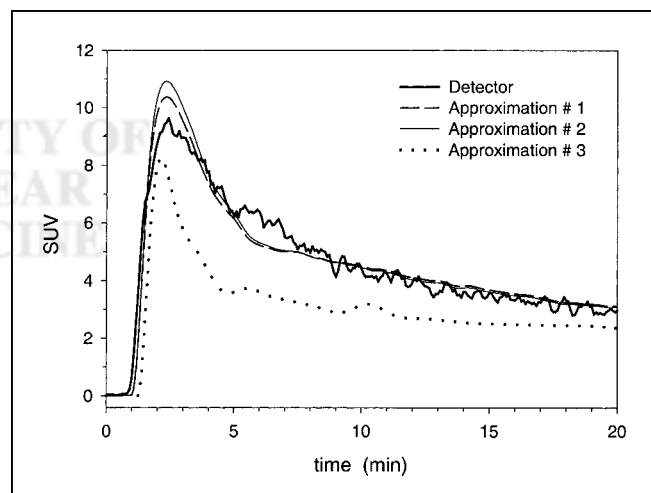


**FIGURE 4.** Approximation of venous input function measured directly in portal vein of foxhound 4 (Table 1) by convolution of arterial input measured by external detector with individual system function (#1), arterial input measured by external detector with average system function (#2), and arterial input determined by PET with average system function (#3). Only first 20 min are shown.

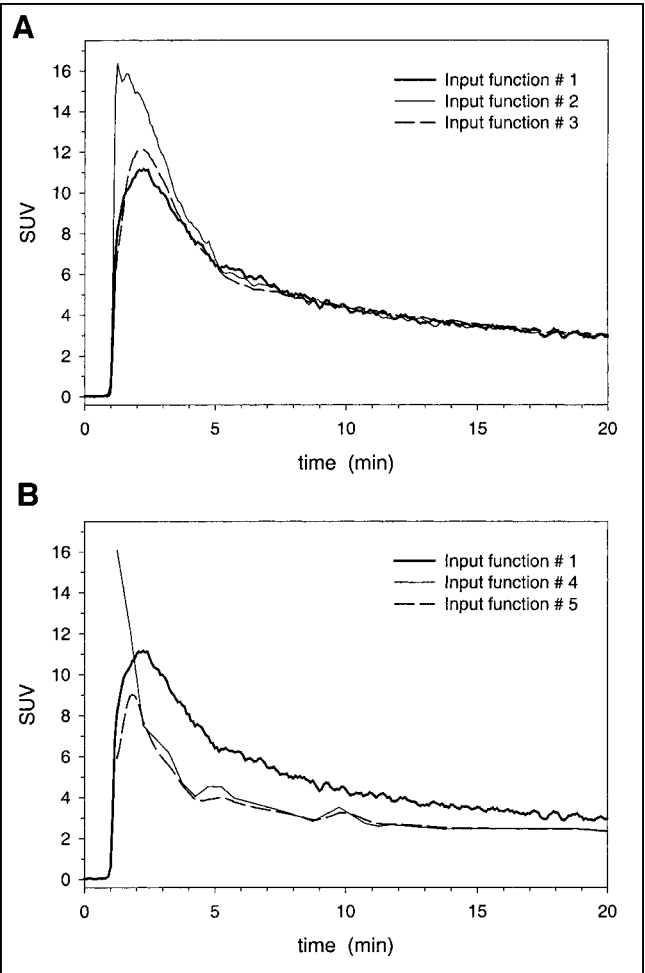


**FIGURE 5.** Comparison of 5 hepatic input functions defined by Equations 2–6 for foxhound 4 (Table 1). Input function #1 is weighted sum of arterial and portal venous blood activities measured by 2 independent external detector systems. Other functions approximate hepatic blood supply by means of arterial activity values obtained from external detector system (A) and from dynamically acquired PET scans (B). Input functions #2 and #4 correspond to single-input model in which hepatic blood supply is described solely by arterial input, whereas input functions #3 and #5 pertain to dual-input scenario in which hepatic input is weighted sum of arterial input and portal venous input estimated by convolving measured arterial time-activity course with average system function  $\bar{S}$  (Fig. 4). Only first 20 min are shown.

each of the 4 rate constants. Therefore, the Wilcoxon and Wilcoxon rank test was used to identify those groups between which significant differences ( $P < 0.05$ ) exist; they are indicated by an asterisk in Figure 7E.

For comparison of the adequacy of the model fits to the liver data using the different input functions, the numeric scores computed on the basis of the Schwarz criterion are shown in Figure 7E. According to this test parameter, input models #1 (mean  $SC$  averaged for the 5 foxhounds,  $SC = -16.3$ ) and #3 ( $SC = -15.2$ ) are slightly superior to input models #2 ( $SC = -2.7$ ) and #5 ( $SC = -9.9$ ). The worst results were obtained for input model #4 ( $SC = 22.6$ ).

## DISCUSSION

In contrast to the arterial input, the portal venous blood supply to the liver cannot be monitored directly by means of dynamic PET measurements because of the inaccessibility of the portal vein on PET scans. We investigated whether the dual hepatic input can be predicted from the measured arterial input. Moreover, the effect of different input models on pharmacokinetic parameters estimated for normal liver tissue was assessed by means of the standard 3-compartment model that describes FDG transport and metabolism.

To this end, an average system function,  $\bar{S}$ , which describes the dispersion of the arterial input on its way through the gastrointestinal tract to the portal vein, was computed by nonlinear regression analysis from arterial and portal venous blood time-activity courses measured separately for 5 dogs by means of 2 extracorporeal detector loops. The system function predicts the time-activity course at the portal vein for an instantaneous arterial input. Consequently, the first moment of this function—the mean transit time,  $MTT$ —is the average time

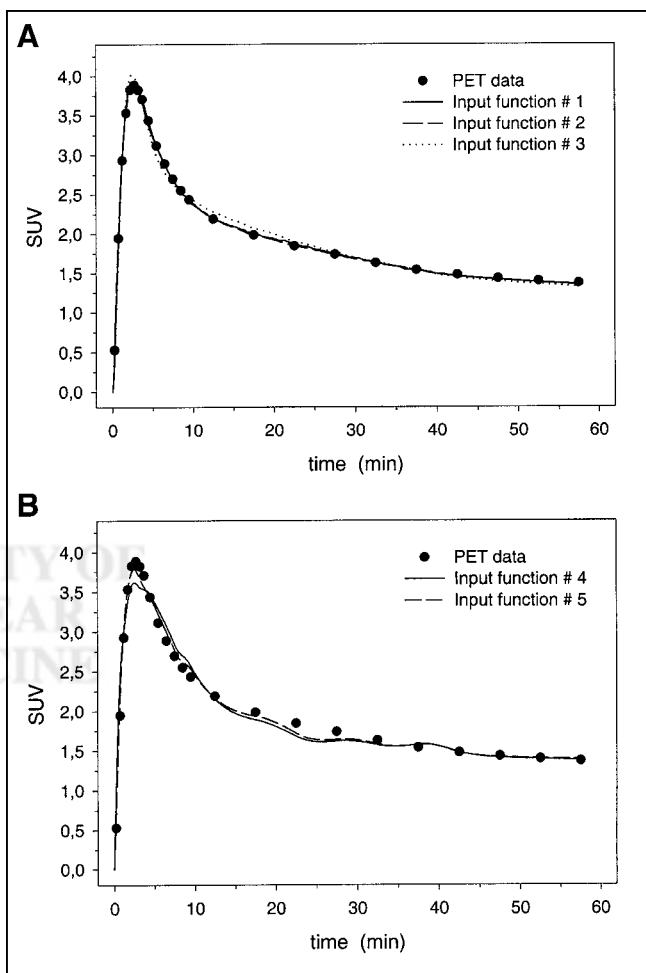


**FIGURE 6.** SUVs measured dynamically by PET from normal liver tissue of foxhound 4. Curves show 3-compartment model fits computed for input models #1–#3 estimated from external blood activity measurements (A) and input models #4 and #5 estimated from blood activity measurements with PET (B).

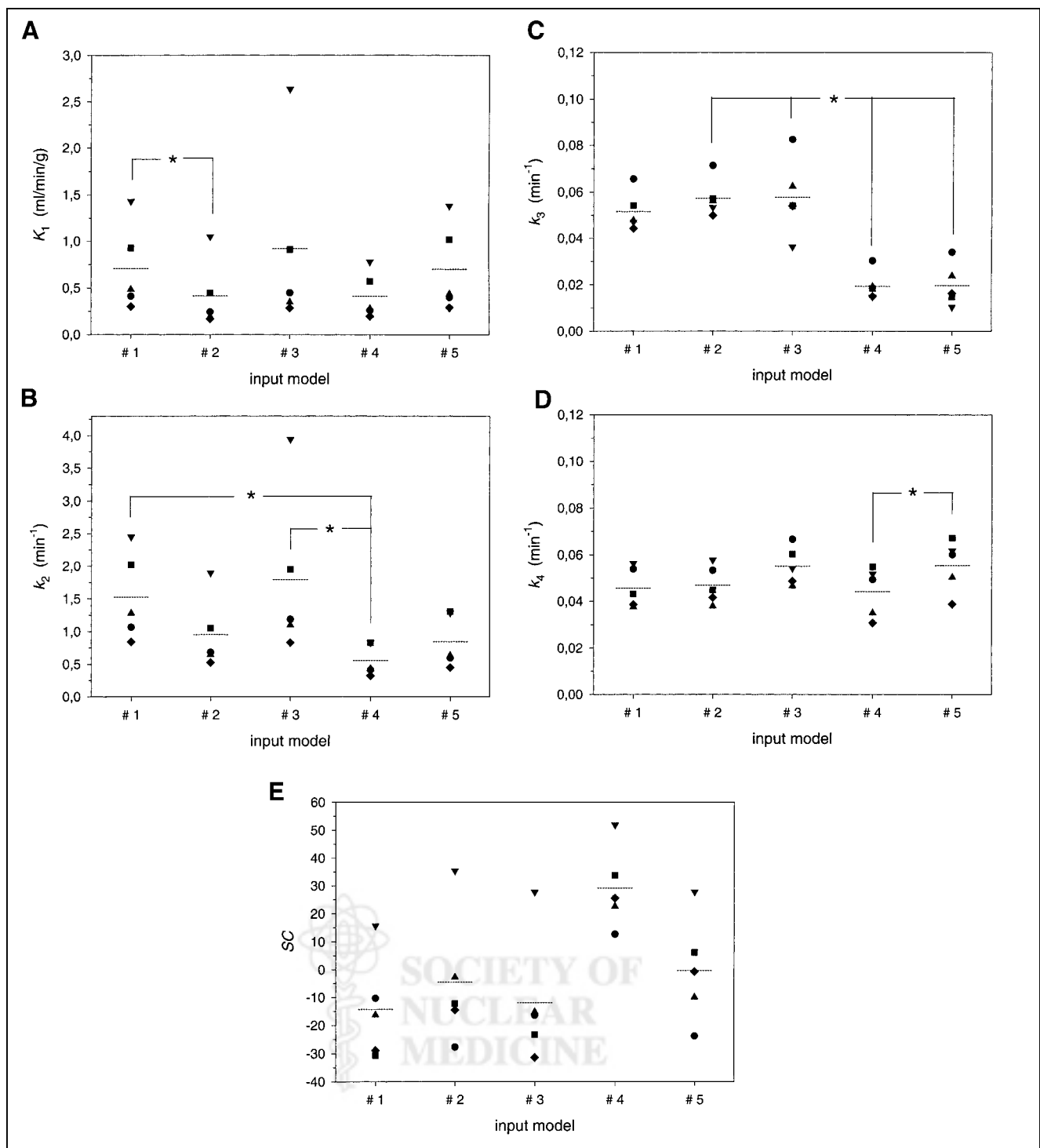


**FIGURE 7.** Effect of 5 different input models defined by Equations 2–6 on pharmacokinetic parameter estimates for 3-compartment model characterizing transport and metabolism of FDG in normal liver. (A)  $K_1$ . (B)  $k_2$ . (C)  $k_3$ . (D)  $k_4$ . Significant differences ( $P < 0.05$ ) between pairs of parameter distributions are marked by asterisk. (E) Numeric scores computed in accordance with Schwarz criterion to compare adequacy of model fits to liver data using different input models. Symbols show individual fit values; horizontal lines indicate corresponding mean values.

required for the tracer molecules to pass from the aorta to the portal vein (11). For the foxhounds, a reasonable mean value of  $MTT_f = 25$  s was obtained from the dominant fast component of the estimated average system function (Eq. 1 and Fig. 3).

There are 3 problems with the approach presented: (a) The measured portal blood curve may not exactly resemble the true portal input to the liver. For example, if the portal catheter is not positioned close enough to the liver, then not

all of the venous blood draining into the portal vein will be measured. Consequently, the recorded portal input will be less than the real input. Any measurement of portal concentrations will be hampered by this effect. (b) To compute the system function, it was assumed that the dispersion of the arterial and portal venous input functions in the extracorporeal detector loops is identical. (c) The portal venous input is approximated by means of an average system function and, thus, interindividual variations are not considered as indicated in Table 1. In relation to our data, however, this approximation has no significant effect on the adequacy of the model fits to the liver data (input model #1,  $SC = -16.3$ ; input model #3,  $\bar{SC} = -15.2$ ) and on the fitted rate constants (Fig. 7).

In clinical routine, measurement of time–activity courses from arterial blood by successive blood sampling causes discomfort to the patient and adds to the radiation burden of the PET staff (29). Therefore, many investigators have tried to replace arterial blood sampling by the noninvasive determination of time–activity courses from either the left ventricle or the abdominal aorta visualized on dynamically acquired PET scans (3,29–31). This approach requires that partial-volume effects be corrected carefully. According to our results, the dual blood supply to the liver can be sufficiently well approximated by means of the weighted sum of the arterial input function determined by dynamic PET scanning from the abdominal aorta and a portal venous input estimated by convolving this function with the average system function  $\bar{S}$  (input model #5). Although the adequacy of the model fits to the liver data for this approximation was slightly inferior ( $\bar{SC} = -9.9$ ) in relation to the reference model #1 ( $SC = -16.3$ ), we did not find significant differences between the corresponding rate constants. In contrast, approximation of the hepatic blood supply solely by means of the measured arterial input function (model #4) as suggested by Choi et al. (12) yielded an inferior parameterization of the measured liver data ( $SC = 22.6$ ) along with significantly ( $P < 0.05$ ) lower  $k_2$  rates compared with model #1 (Fig. 7B).

For the 3 input models #1, #3, and #5, which correspond to a dual-input scenario, mean values of 0.71, 0.93, and 0.71 mL/min/g, respectively, were obtained for the rate constant  $K_1$  representing total liver blood flow (12). These values are in close agreement with a hepatic blood flow of 0.93 mL/min/g determined for the same foxhounds by means of a standard microsphere technique (19). On the other hand, lower mean  $K_1$  rates of 0.42 and 0.41 mL/min/g were obtained for the single-input models #2 and #4, respectively.

After a strong initial FDG uptake, the time–activity courses measured in the normal liver (Fig. 6) showed a rapid clearance of the radioactivity. This effect reflects the back diffusion of free FDG from the hepatocytes into blood plasma associated with a low phosphorylation rate ( $k_3$ ; Fig. 7C) and a high dephosphorylation rate ( $k_4$ ; Fig. 7D) (32). On

the basis of the liver data measured in our study, a relatively high  $k_4$  value of  $0.05 \pm 0.01 \text{ min}^{-1}$  was determined, which is consistent with the high level of glucose-6-phosphatase present in normal liver tissue (9).

None of the input models investigated in this study provides a wholly satisfactory representation of the complex hepatic blood supply in normal liver tissue from a methodologic point of view. However, our data indicate that dual-input models are superior to the corresponding single-input models with respect to approximation of the acquired liver data and estimation of reliable rate constants. Moreover, our analysis reveals that differences between the rate constants estimated for the 3 different dual-input models (models #1, #3, and #5) were smaller than interindividual variations within the different model groups. Thus, it can be concluded that the estimation of rate constants as defined by the standard 3-compartment FDG model is a relatively robust procedure in relation to uncertainties in the hepatic input function. For a quantitative analysis of FDG uptake in the normal liver, we thus recommend approximation of the portal venous input by convolution of the measured arterial input with an average system function. For humans, this function may be estimated from dynamic MRI studies using a suitable paramagnetic contrast agent (33).

On the other hand, with regard to FDG PET examinations of patients with liver disease, it must be considered that malignant and benign lesions of the liver are—in contrast to healthy liver tissue—supplied mainly with blood by the hepatic artery (34–39). Taking this fact into account, it seems to be a reasonable approach for clinical FDG PET studies on patients with liver lesions to approximate the hepatic input function by means of the time–activity course determined noninvasively from the left ventricle or the abdominal aorta visualized on dynamically acquired PET scans.

However, the quantitative analysis of dispersion effects in the gastrointestinal tract presented in this study is of importance not only for FDG modeling but also for the development and evaluation of realistic biokinetic blood circulation and alimentary tract models. Such models are currently undergoing investigation by the International Commission on Radiological Protection to improve internal dosimetry for radiopharmaceuticals labeled with short-lived radionuclides (such as  $^{15}\text{O}$ -labeled water) (40).

## CONCLUSION

Dual-input models proved to be superior to single-input models with respect to the adequacy of FDG model fits to normal liver data. According to our data, the portal venous input to the liver can be sufficiently well approximated by convolving the measured arterial input function with an average system function that describes the dispersion of the arterial input on its way through the gastrointestinal tract to the portal vein. However, for evaluation of the kinetics of

FDG uptake in liver lesions that are supplied largely by the hepatic artery, it seems to be valid to approximate the hepatic blood supply by the arterial input function.

## ACKNOWLEDGMENTS

The authors gratefully acknowledge the technical support of Herbert Trojan and also thank Annemarie Theobald, Werner Konowalczuk, and Heike Marx for providing the radiopharmaceuticals.

## REFERENCES

- Okazumi SO, Isono K, Enomoto K, et al. Evaluation of liver tumors using fluorine-18-fluorodeoxyglucose PET: characterization of tumor and assessment of effect of treatment. *J Nucl Med*. 1992;33:333–339.
- Messa C, Choi Y, Hoh CK, et al. Quantification of glucose utilization in liver metastases: parametric imaging of FDG uptake with PET. *J Comput Assist Tomogr*. 1992;16:684–689.
- Torizuka T, Tamaki N, Inokuma T, et al. In vivo assessment of glucose metabolism in hepatocellular carcinoma with FDG-PET. *J Nucl Med*. 1995;36:1811–1817.
- Delbeke D, Martin WH, Sandler MP, Chapman WC, Wright K, Pinson CW. Evaluation of benign vs malignant hepatic lesions with positron emission tomography. *Arch Surg*. 1998;133:510–516.
- Hustin R, Paulus P, Jacquet N, Jerusalem G, Bury T, Rigo P. Clinical evaluation of whole-body <sup>18</sup>F-fluorodeoxyglucose positron emission tomography in the detection of liver metastases. *Ann Oncol*. 1998;9:397–401.
- Trojan J, Schroeder O, Raedle J, et al. Fluorine-18 FDG positron emission tomography for imaging of hepatocellular carcinoma. *Am J Gastroenterol*. 1999;94:3314–3319.
- Bender H, Bangard N, Metten N, et al. Possible role of FDG-PET in the early prediction of therapy outcome in liver metastases of colorectal cancer. *Hybridoma*. 1999;18:87–91.
- Delbeke D. Oncological applications of FDG PET imaging. *J Nucl Med*. 1999;40:1706–1715.
- Weber G, Cantero A. Glucose-6-phosphatase activity in normal, precancerous, and neoplastic tissues. *Cancer Res*. 1955;15:105–108.
- Weber G, Morris HP. Comparative biochemistry of hepatomas. III. Carbohydrate enzymes in liver tumors of different growth rates. *Cancer Res*. 1963;23:987–994.
- Peters AM, Myers MJ. *Physiological Measurements with Radionuclides in Clinical Practise*. Oxford, U.K.: Oxford University Press; 1998.
- Choi Y, Hawkins RA, Huang SC, et al. Evaluation of the effect of glucose ingestion and kinetic model configurations of FDG in the normal liver. *J Nucl Med*. 1994;35:818–823.
- Oberdorfer F, Hull WE, Traving BC, Maier-Borst W. Synthesis and purification of 2-deoxy-2-[<sup>18</sup>F]fluoro-D-glucose and 2-deoxy-2-[<sup>18</sup>F]fluoro-D-mannose: characterization of products by <sup>1</sup>H- and <sup>19</sup>F-NMR spectroscopy. *Int J Rad Appl Instrum [A]*. 1986;37:695–701.
- Holte S, Ostertag H, Kesselberg M. A preliminary evaluation of a dual crystal positron camera. *J Comput Assist Tomogr*. 1987;11:691–697.
- Eriksson L, Holte S, Bohm C, Kesselberg M, Hovander B. Automated blood sampling systems for positron emission tomography. *IEEE Trans Nucl Sci*. 1988;35:703–707.
- Hoverath H, Kübler WK, Ostertag HJ, et al. Scatter correction in the transaxial slices of a whole-body positron emission tomograph. *Phys Med Biol*. 1993;38:717–728.
- Brix G, Doll J, Bellemann ME, et al. Use of scanner characteristics in iterative image reconstruction for high-resolution positron emission tomography studies of small animals. *Eur J Nucl Med*. 1997;24:779–786.
- Schoenberg SO, Just A, Kallinowski F, Bock M. Correlation of hemodynamic impact and morphologic degree of renal artery stenosis in a canine model. *J Am Soc Nephrol*. 2000;11:2190–2198.
- Ziegler SI, Haberkorn U, Byrne H, et al. Measurement of liver blood flow using oxygen-15 labelled water and dynamic positron emission tomography: limitations of model description. *Eur J Nucl Med*. 1996;23:169–177.
- Bellemann ME, Haberkorn U, Brix G, Gerlach L, Lorenz WJ. Measurement of the arterial input function at high temporal resolution in dynamic PET [abstract]. *J Nucl Med*. 1996;37(suppl):266P.
- Haberkorn U, Bellemann ME, Altmann A, et al. PET of 2-fluoro-2-deoxyglucose uptake in rat prostate adenocarcinoma during chemotherapy with gemcitabine. *J Nucl Med*. 1997;38:1215–1221.
- Phelps ME, Huang SC, Hoffman EJ, Selin C, Sokoloff L, Kuhl DE. Tomographic measurement of local cerebral glucose metabolic rate in humans with (F-18)2-fluoro-2-deoxy-D-glucose: validation of method. *Ann Neurol*. 1997;6:371–388.
- Huang SC, Phelps ME, Hoffman EJ, Sideris K, Selin CJ, Kuhl DE. Noninvasive determination of local cerebral metabolic rate of glucose in man. *Am J Physiol*. 1980;238:E69–E82.
- D'Argenio DZ, Schmitzky A. *ADAPT II User's Guide: Pharmacokinetic/Pharmacodynamic Systems Analysis Software*. Los Angeles, CA: Biomedical Simulation Resource, University of Southern California; 1997.
- Schwarz G. Estimating the dimension of a model. *Ann Stat*. 1978;6:461–564.
- Sachs L. *Applied Statistics* [in German]. Berlin, Germany: Springer-Verlag; 1997.
- Wilcoxon F, Wilcox RA. *Some Rapid Approximate Statistical Procedures*. Pearl River, NY: Lederle Laboratories; 1994:36–38.
- Blustajn J, Cuenod CA, Clement O, Siauve N, Vuillemin-Bodaghi V, Frija G. Measurement of liver blood volume using a macromolecular MRI contrast agent at equilibrium. *Magn Reson Imaging*. 1997;15:415–421.
- Keiding S, Munk OL, Schiøtt KM, Hansen SB. Dynamic 2-[<sup>18</sup>F]fluoro-2-deoxy-D-glucose positron emission tomography of liver tumours without blood sampling. *Eur J Nucl Med*. 2000;27:407–412.
- Germano G, Chen BC, Huang SC, Gambhir SS, Hoffman EJ, Phelps ME. Use of the abdominal aorta for arterial input function determination in hepatic and renal PET studies. *J Nucl Med*. 1992;33:613–620.
- Kissel J, Port R, Zaers J, et al. Noninvasive determination of the arterial input function of an anticancer drug from dynamic PET scans using the population approach. *Med Phys*. 1999;26:609–615.
- Gallagher BM, Fowler JS, Guttersen NI, MacGregor RR, Wan CN, Wolf AP. Metabolic trapping as a principle of radiopharmaceuticals design: some factors responsible for the biodistribution of [<sup>18</sup>F]2-deoxy-2-fluoro-D-glucose. *J Nucl Med*. 1978;19:1154–1161.
- Hoffmann U, Brix G, Scharf J, Lorenz WJ. Quantitative analysis of the portal and arterial blood supply of liver lesions by means of dynamic MRI. *Proc Int Soc Magn Reson Med*. 1997;3:2083.
- Breedis C, Young G. The blood supply of neoplasms in the liver. *Am J Pathol*. 1954;30:969–985.
- Biersack HJ, Torres J, Thelen M, Monzon O, Winkler C. Determination of liver and spleen perfusion by quantitative sequential scintigraphy: results in normal subjects and in patients with portal hypertension. *Clin Nucl Med*. 1981;6:218–220.
- McLean AJ, Morgan DJ. Clinical pharmacokinetics in patients with liver disease. *Clin Pharmacokinet*. 1991;1:42–69.
- Marti-Bonmati L, Masia L, Torrijo C, Casillas C, Ferrer MD. Dynamic MR imaging of liver tumors: analysis with temporal reconstruction images. *Radiology*. 1994;193:677–682.
- Hoffmann U, Brix G, Scharf J, Knopp MV, Lorenz WJ. Dynamic MRT of the liver. *Proc Int Soc Magn Reson Med*. 1995;1:1471.
- el-Khalily H, Hoeffken H, von Wichert P, Joseph K. Hepatic perfusion scintigraphy: relation of liver perfusion and ascites in patients with liver cirrhosis. *Clin Nucl Med*. 1996;21:132–135.
- Métivier H. The work of committee 2 of ICRP on a new model for the human alimentary tract. *Radiat Prot Dosim*. 1999;79:272–277.